NASA/TM—2013-217838 AIAA–2013–0012

Exhaust Nozzle Plume and Shock Wave Interaction

Raymond S. Castner
Glenn Research Center, Cleveland, Ohio

Alaa Elmiligui
Langley Research Center, Hampton, Virginia

Susan Cliff
Ames Research Center, Moffett Field, California

February 2013

NASA STI Program . . . in Profile

Since its founding, NASA has been dedicated to the advancement of aeronautics and space science. The NASA Scientific and Technical Information (STI) program plays a key part in helping NASA maintain this important role.

The NASA STI Program operates under the auspices of the Agency Chief Information Officer. It collects, organizes, provides for archiving, and disseminates NASA's STI. The NASA STI program provides access to the NASA Aeronautics and Space Database and its public interface, the NASA Technical Reports Server, thus providing one of the largest collections of aeronautical and space science STI in the world. Results are published in both non-NASA channels and by NASA in the NASA STI Report Series, which includes the following report types:

- TECHNICAL PUBLICATION. Reports of completed research or a major significant phase of research that present the results of NASA programs and include extensive data or theoretical analysis. Includes compilations of significant scientific and technical data and information deemed to be of continuing reference value. NASA counterpart of peer-reviewed formal professional papers but has less stringent limitations on manuscript length and extent of graphic presentations.

- TECHNICAL MEMORANDUM. Scientific and technical findings that are preliminary or of specialized interest, e.g., quick release reports, working papers, and bibliographies that contain minimal annotation. Does not contain extensive analysis.

- CONTRACTOR REPORT. Scientific and technical findings by NASA-sponsored contractors and grantees.

- CONFERENCE PUBLICATION. Collected papers from scientific and technical conferences, symposia, seminars, or other meetings sponsored or cosponsored by NASA.

- SPECIAL PUBLICATION. Scientific, technical, or historical information from NASA programs, projects, and missions, often concerned with subjects having substantial public interest.

- TECHNICAL TRANSLATION. English-language translations of foreign scientific and technical material pertinent to NASA's mission.

Specialized services also include creating custom thesauri, building customized databases, organizing and publishing research results.

For more information about the NASA STI program, see the following:

- Access the NASA STI program home page at *http://www.sti.nasa.gov*

- E-mail your question to *help@sti.nasa.gov*

- Fax your question to the NASA STI Information Desk at 443–757–5803

- Phone the NASA STI Information Desk at 443–757–5802

- Write to:
  STI Information Desk
  NASA Center for AeroSpace Information
  7115 Standard Drive
  Hanover, MD 21076–1320

NASA/TM—2013-217838 AIAA–2013–0012

Exhaust Nozzle Plume and Shock Wave Interaction

Raymond S. Castner
Glenn Research Center, Cleveland, Ohio

Alaa Elmiligui
Langley Research Center, Hampton, Virginia

Susan Cliff
Ames Research Center, Moffett Field, California

Prepared for the
51st Aerospace Science Conference
sponsored by the American Institute of Aeronautics and Astronautics
Grapevine, Texas, January 7–10, 2013

National Aeronautics and
Space Administration

Glenn Research Center
Cleveland, Ohio 44135

February 2013

Acknowledgments

This work was funded by the NASA Fundamental Aeronautics Program, High Speed Project.

This work was sponsored by the Fundamental Aeronautics Program at the NASA Glenn Research Center.

Level of Review: This material has been technically reviewed by technical management.

Available from

NASA Center for Aerospace Information
7115 Standard Drive
Hanover, MD 21076–1320

National Technical Information Service
5301 Shawnee Road
Alexandria, VA 22312

Available electronically at http://www.sti.nasa.gov

Exhaust Nozzle Plume and Shock Wave Interaction

Raymond S. Castner
National Aeronautics and Space Administration
Glenn Research Center
Cleveland, Ohio 44135

Alaa Elmiligui
National Aeronautics and Space Administration
Langley Research Center
Hampton, Virginia 23681

Susan Cliff
National Aeronautics and Space Administration
Ames Research Center
Moffett Field, California 94035

Abstract

Fundamental research for sonic boom reduction is needed to quantify the interaction of shock waves generated from the aircraft wing or tail surfaces with the exhaust plume. Both the nozzle exhaust plume shape and the tail shock shape may be affected by an interaction that may alter the vehicle sonic boom signature. The plume and shock interaction was studied using Computational Fluid Dynamics simulation on two types of convergent-divergent nozzles and a simple wedge shock generator. The nozzle plume effects on the lower wedge compression region are evaluated for two- and three-dimensional nozzle plumes. Results show that the compression from the wedge deflects the nozzle plume and shocks form on the deflected lower plume boundary. The sonic boom pressure signature of the wedge is modified by the presence of the plume, and the computational predictions show significant (8 to 15 percent) changes in shock amplitude.

Nomenclature

AOA	Angle of attack, degrees
β	Nozzle boat-tail angle, degrees
D	Test nozzle diameter, in.
h	Distance below vehicle, in.
L	Vehicle length, in.
M_∞	Free-stream Mach number
NPR	Nozzle pressure ratio = P_t / P_∞
P	Local static pressure, psia
P_t	Total pressure in nozzle, psia
P_∞	Free-stream static pressure, psia
ΔP	$P - P_\infty$
$\Delta P/P$	$(P - P_\infty)/ P_\infty$
T_o	Nozzle total temperature, R
T_∞	Free-stream total temperature, R
t	Time, seconds
x	Distance along abscissa of pressure signature, in.
y	Vertical distance from nozzle centerline, in.

Introduction

The reduction of sonic boom overpressures of supersonic aircraft may enable high speed travel over populated areas. The impact of the sonic boom on populated areas is so large that the FAA has prohibited supersonic flight over land by civil aircraft in the United States. Most supersonic aircraft produce an N-wave pressure signature on the ground; a rise in pressure from the bow shock of the vehicle followed by an expansion to a negative pressure and then the return to atmospheric pressure. The bow and tail shocks create the "double boom" often heard on the ground. The aircraft pressure signature near the vehicle has multiple shocks and expansions that attenuate and coalesce to the N-wave form on the ground.

Recent studies to develop aircraft with acceptable sonic boom noise include programs such as the Quiet Spike (Ref. 1) and the Shaped Sonic Boom Demonstrator (SSBD) (Ref. 2) that achieved reduced intensity of the forward portion of the pressure signature. Research was also done to reduce the loudness contribution from aft components including the nozzle exhaust. One example was the work of Putnam (Ref. 3), who performed an experimental study of exhaust nozzles and the effects of the exhaust plume. Tests were done in a 4- by 4-ft supersonic wind tunnel with pressure measurements taken one diameter away from the nozzle. Study of exhaust nozzle plume effect on sonic boom has progressed from analysis and testing of an isolated nozzle (Refs. 4 and 5), to slot nozzles (Ref. 6) and engine-wing-body models (Refs. 7 and 8). These studies demonstrated how the nozzle lip shock from an under-expanded nozzle plume could suppress the nozzle boat-tail expansion and reduce the trailing shock.

The previous studies did not examine the exhaust nozzle plume interaction with shocks generated by the wing and tail, which may affect the plume shape and the sonic boom signature. The subject of this report is the study of simplified exhaust nozzle plume interaction with a tail shock, generated by a simple wedge shock generator (wedge). The intent is to provide a baseline analysis of a generic nozzle and wedge configuration, and demonstrate the effect of the nozzle exhaust plume on the wedge pressure signature. The WIND-US, PAB3D, Cart3D, and USM3D computational fluid dynamic (CFD) codes were used for this analysis. Two types of supersonic nozzle plumes were studied: one created by a two-dimensional (2-D) convergent-divergent (CD) slot nozzle and one created by an axisymmetric CD nozzle (Putnam's "Nozzle 6"). The axisymmetric CD nozzle was also studied within the aft fuselage of a 59° delta wing-body model. CFD codes and geometry models are listed in Table I. The Mach number contours and pressure profiles from these configurations are presented.

Computational Modeling

WIND-US

Two- and three-dimensional (3-D) exhaust nozzles were modeled with WIND-US (Table I). WIND-US is a general purpose fluid flow solver that is used to numerically solve various sets of equations governing physical phenomena (Ref. 9). WIND-US was used to take advantage of the established capability to correctly compute nozzle plumes with viscous and turbulence effects. The code supports the solution of the Euler and Navier-Stokes equations, along with supporting equation sets governing turbulent and chemically-reacting flows. The flow solver is parallelized and can take advantage of multi-core and multi-CPU hardware. The version used was WIND-US 4.6. WIND-US was used with the modified second-order Roe upwind scheme for stretched grids, implicit time stepping with a Courant–Friedrichs–Lewy (CFL) number of 1.0, and the Menter Shear Stress Transport (SST) turbulence model.

PAB3D

In this study, PAB3D (Ref. 10) was used in conjunction with two-equation k–ε turbulence closure and nonlinear algebraic Reynolds stress models to simulate the 2-D CD supersonic nozzle (Table I). PAB3D has been tested and documented for the simulation of aero-propulsive and aerodynamic flows involving separation, mixing, and other complicated phenomena. PAB3D has been ported to a number of platforms,

and offers a combination of good performance and low memory requirements. In addition to its advanced preprocessor, which can handle complex geometries through multi-block general patching, PAB3D has a runtime module capable of calculating aerodynamic performance and a postprocessor for data analysis (Ref. 11). PAB3D solves the simplified Reynolds-averaged Navier–Stokes equations in conservative form by neglecting streamwise derivatives of the viscous terms. Viscous models include coupled and uncoupled simplified Navier–Stokes and thin-layer Navier–Stokes solver options. Roe's upwind scheme is used to evaluate the explicit part of the governing equations, and van Leer's scheme is used for the implicit part. Diffusion terms are centrally differenced, inviscid terms are upwind differenced, and two finite volume flux-splitting schemes are used to construct the convective flux terms. PAB3D is third order accurate in space and second-order accurate in time.

TABLE I.—SUMMARY OF CFD CODES AND GEOMETRY MODELS

CFD Code	Geometry	
	2-D Models	3-D Models
WIND-US	2-D CD Supersonic Slot Nozzle	3-D Axisymmetric CD "Nozzle 6"
PAB3D	2-D CD Supersonic Slot Nozzle	----------
Cart3D	----------	59° Wing-body Model with "Nozzle 6"
USM3D	----------	59° Wing-body Model with "Nozzle 6"

Cart3D

Cart3D was used to evaluate 3-D effects for a 59° delta wing-body model with a fuselage embedded CD nozzle and a wedge shock located above the nozzle plume (Table I). Cart3D (Refs. 12 and 13) is a high-fidelity analysis package for conceptual and preliminary aerodynamic design that provides solution to the Euler equations. It allows users to perform automated CFD analysis on complex geometry. Geometry for Cart3D is represented by surface triangulations. These may be generated from within a Computer-Aided Design (CAD) system, from legacy surface triangulations or from diagonalized (diagonal added to each quadrilateral face) structured surface grids. Cart3D uses an embedded multilevel Cartesian mesh to discretize the space surrounding the geometry and determines the surface geometry out of the set of "cut-cells" which intersect the surface triangulation. The flow solver is parallelized via OPENMP and can take advantage of multi-core and multi-CPU hardware. Solutions were obtained using the adjoint-based mesh adaptation module (Refs. 14 to 16). This module uses adjoint-weighted residual error-estimates to drive mesh adaptation. Once a user specifies the output function of interest, such as lift, drag, or off-body pressures along a line with a corresponding error tolerance; the module automatically refines the mesh to drive the remaining numerical errors below the requested tolerance. This module combined with domain rotation to nearly align the mesh with the Mach angle has been validated for sonic boom prediction by Wintzer (Ref. 17) and others with and without adaptation (Refs. 18 to 21). The adaptation module allows greatly reduced mesh generation and analysis time and offers effective use of computational resources for an accurate solution.

USM3D

The 59° delta wing-body model with the embedded fuselage CD nozzle was also studied using USM3D (Table I). USM3D is a tetrahedral cell-centered, finite volume Euler and Navier-Stokes (N-S) method. The USM3D flow solver has a variety of options for solving the flow equations and several turbulence models for closure of the N-S equations (Refs. 22 and 23). For the current study, Roe's flux difference splitting scheme was used and the CFL was set to 20. Flux limiters are used within the code to preclude oscillations due to shocks and discontinuities by limiting the values of the spatial derivatives. For the present study, at the start of a new solution, the USM3D code was computed using the Spalart-Allmaras turbulence model with first order spatial accuracy for 10000 iterations, and then the code automatically switched to second order spatial accuracy. Obtaining a well-converged first order accurate solution before switching to 2nd order significantly improves the chance of convergence with the code, but

it is sometimes not necessary. USM3D has been used for propulsion simulation and plume induced flow separation studies (Refs. 24 and 25). The present study implements a simplified approach to generate a nozzle exhaust plume. The CD solid nozzle shape developed by Putnam was modeled within the aft fuselage of the 59° delta wing-body configuration. The boundary condition at the nozzle plenum face was set to a cold air jet temperature of 590 °R, and a pressure of 8 times atmospheric conditions at 50,000 ft. The ratio of specific heats was assumed 1.4 within the nozzle as well as in the free-stream flowfield.

Geometry Modeling

2-D CD Supersonic Slot Nozzle: WIND-US and PAB3D

For the 2-D supersonic slot nozzle, both WIND-US and PAB3D utilized the same grid. A structured computational domain consisting of 13 zones and 461,496 grid points was used (Figure 1). This nozzle geometry simulates a high aspect ratio slot nozzle with infinite span. Simulations were run at the design nozzle pressure ratio (NPR) of 8.0. Temperature for the nozzle plume was 530 °R, with one case run at 1900 °R for the 5° wedge. Critical dimensions for the nozzle were a 2.05 in. throat height and a 3.88 in. exit height; the boat-tail angle was 5°, with a 2.6 in. long boat-tail bevel (Figure 1(a)). The computational domain extended 152 in. downstream of the nozzle exit, 22.86 in. above, and 45.7 in. below the nozzle (Figure 1(b)). Multi-block wall-packed grids, with the initial grid spacing producing y^+ values near 1.0, were generated for use on parallel processor systems. Viscous wall boundaries were used for all nozzle surfaces. Convergence was assessed by monitoring the nozzle mass flow and the off-body pressure profile at 12.5 in. below the centerline of the nozzle. External flow conditions were run at Mach 2.2, an angle of attack of 0° for a 50,000 ft flight altitude.

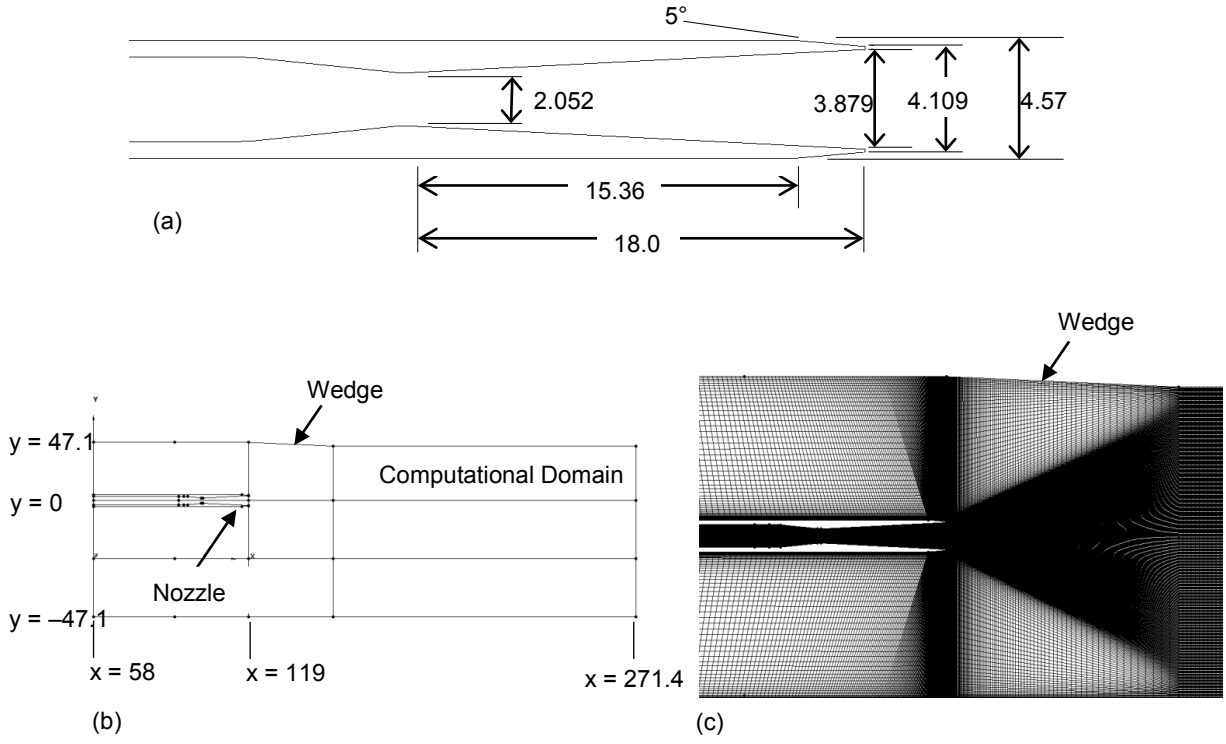

Figure 1.—(a) 2-D CD supersonic slot nozzle geometry, (b) computational domain for the 2-D CD supersonic slot nozzle with a 2.5° wedge angle, and (c) details of grid at nozzle exit.

The wedge shock generator (wedge) used in this study had both a 2.5° and 5° half-angle leading edge. The wedge was located 22.86 in. above the nozzle centerline, and the leading edge of the wedge was located at the same axial station as the nozzle exit. The upper boundary of the mesh contains the profile of the lower wedge surface where the boundary conditions were a solid wall with no slip. Boundary conditions upstream and downstream of the wedge were 'freestream' boundaries, as were boundaries at the front, bottom, and aft portion of the computational domain. In WIND-US, 'freestream' boundaries create partial shock reflections, which can only be avoided by moving the boundary farther away from the model, and increasing computational grid size. In this case, the modeling approach was acceptable because the partial shock reflections from the 'freestream' boundaries affected the flow field aft of the shock/nozzle plume interaction at the supersonic flow conditions.

CFD grids were also constructed with a 2.5° and a 5.0° wedge-only components. These solutions were compared to solutions with the wedge and the 2-D CD supersonic slot nozzle.

3-D Axisymmetric CD Supersonic "Nozzle 6": WIND-US

Figure 2(a) displays the seven variations of the axisymmetric CD supersonic exhaust nozzle, as tested by Putnam (Ref. 5). For this study, a scale replica of the sixth design, "Nozzle 6", was selected, as this nozzle is consistent with previous work (Ref. 4). This simulation was run as half of the nozzle with a vertical symmetry plane and consisted of 19 zones with 11,061,540 grid points. This nozzle had a design pressure ratio of 8.12 and simulations were performed at NPR=8. Critical dimensions for the nozzle were a 10.22 in. throat diameter and a 13.42 in. exit diameter; the boat tail angle was 5°. The computational domain (Figure 2(b) and (c)) extended 271 in. downstream of the nozzle exit, and 57.1 in. above and below the nozzle. Multi-block wall-packed grids with the initial grid spacing selected to produce $y^+=1.0$ were generated for use on parallel processor systems. To reduce computational time on a large 3-D grid, inviscid wall boundaries were used for all nozzle surfaces. External flow conditions were run at Mach 2.2, an angle of attack of zero, and an Euler solution was generated.

The wedge (Figure 3) was unswept with 2.5° half angle leading and trailing edges. This wedge permitted study of shock and expansion regions passing through a nozzle plume. The wedge was located at 57.1 in. above the nozzle centerline, and the leading edge of the wedge was located in a plane 13.14 in. upstream of the nozzle exit. In this case, the axial station for the leading edge of the wedge was close to the nozzle throat, not the nozzle exit. The upper boundary of the mesh contained the profile of the lower wedge surface where the boundary conditions were inviscid wall boundaries. All other boundary conditions were again set to the WIND-US 'freestream' boundary condition.

59° Wing-Body Model with "Nozzle 6": Cart3D

The Cart3D model surface (Figure 4(a)) was developed from the baseline "Nozzle 6" paired with the 59° delta-wing body model (Ref. 9). The nozzle flowfield was simulated with a pressure boundary at the nozzle plenum, and Cart3D computations of the nozzle plume were obtained at a nozzle pressure ratio of 8. The computational domain extended 10 body lengths in all directions, and line sensors at both one and two body lengths below the vehicle were used to drive the mesh adaptation.

The wedge used in this test case had a diamond wedge profile with 2.5° half angle leading and trailing edges. The wedge was located 57.1 in. above the nozzle centerline, and the leading edge of the wedge was located in a plane 13.14 in. upstream of the nozzle exit. External flow conditions were run at Mach 2.2 and an angle of attack of zero.

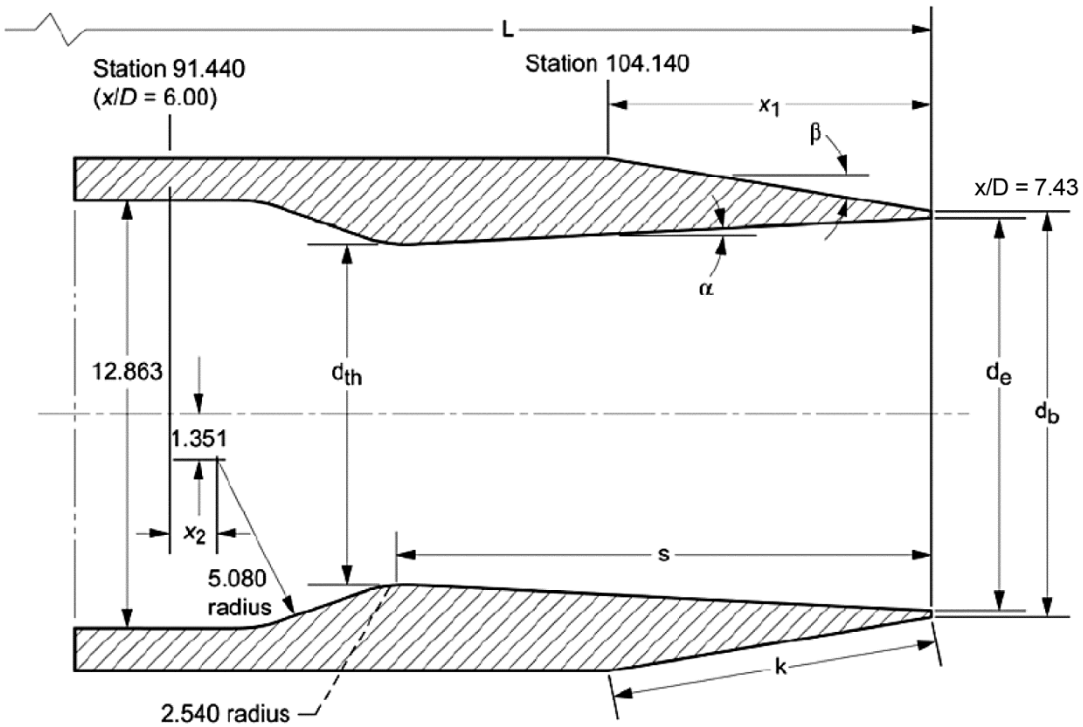

Nozzle	$M_{j,des}$	$(P_{t,j}/P_\infty)_{des}$	α, deg.	β, deg.	x_1	L	k	s	d_{th}	d_e	d_b	A_{th}	A_e	A_e/A_{th}	x_2
1	2.920	32.58	11.50	0	15.240	119.380	15.240	18.519	7.577	15.011	15.240	45.09	176.98	3.925	2.908
2	2.272	11.97	7.28	0	15.240	119.380	15.240	18.747	10.264	15.011	15.240	82.75	176.98	2.139	4.224
3	2.740	24.77	11.50	0	12.192	116.332	12.192	16.878	8.255	15.011	15.240	53.52	176.98	3.307	2.118
4	2.523	17.72	11.50	0	9.144	113.284	9.144	14.883	9.144	15.011	15.240	65.66	176.98	2.695	2.118
5	2.267	11.88	9.06	0	9.144	113.284	9.144	15.011	10.288	15.011	15.240	83.12	176.98	2.129	1.953
6	2.024	8.12	6.04	5	9.109	113.249	9.144	15.105	10.223	13.417	13.646	82.08	141.39	1.722	1.778
7	1.700	4.94	3.04	10	8.999	113.139	9.144	15.166	10.231	11.836	12.065	82.21	110.03	1.338	1.580

(a)

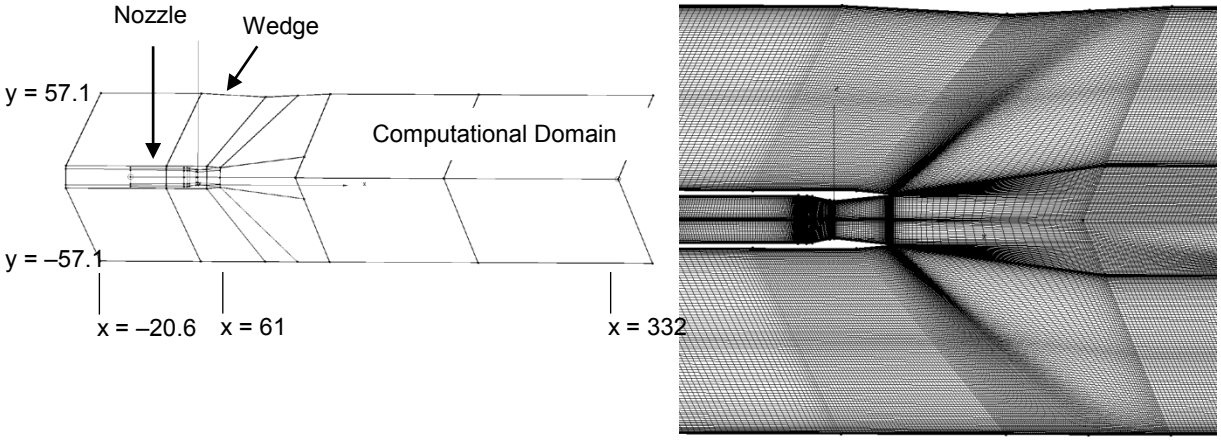

(b)

Figure 2.—(a) Three-dimensional axisymmetric CD supersonic “Nozzle 6” from Putnam (Ref. 3), (b) computational domain (centerline cut) for 3-D axisymmetric CD supersonic ‘Nozzle 6’ with the 2.5° wedge angle, (c) grid at nozzle exit (centerline cut).

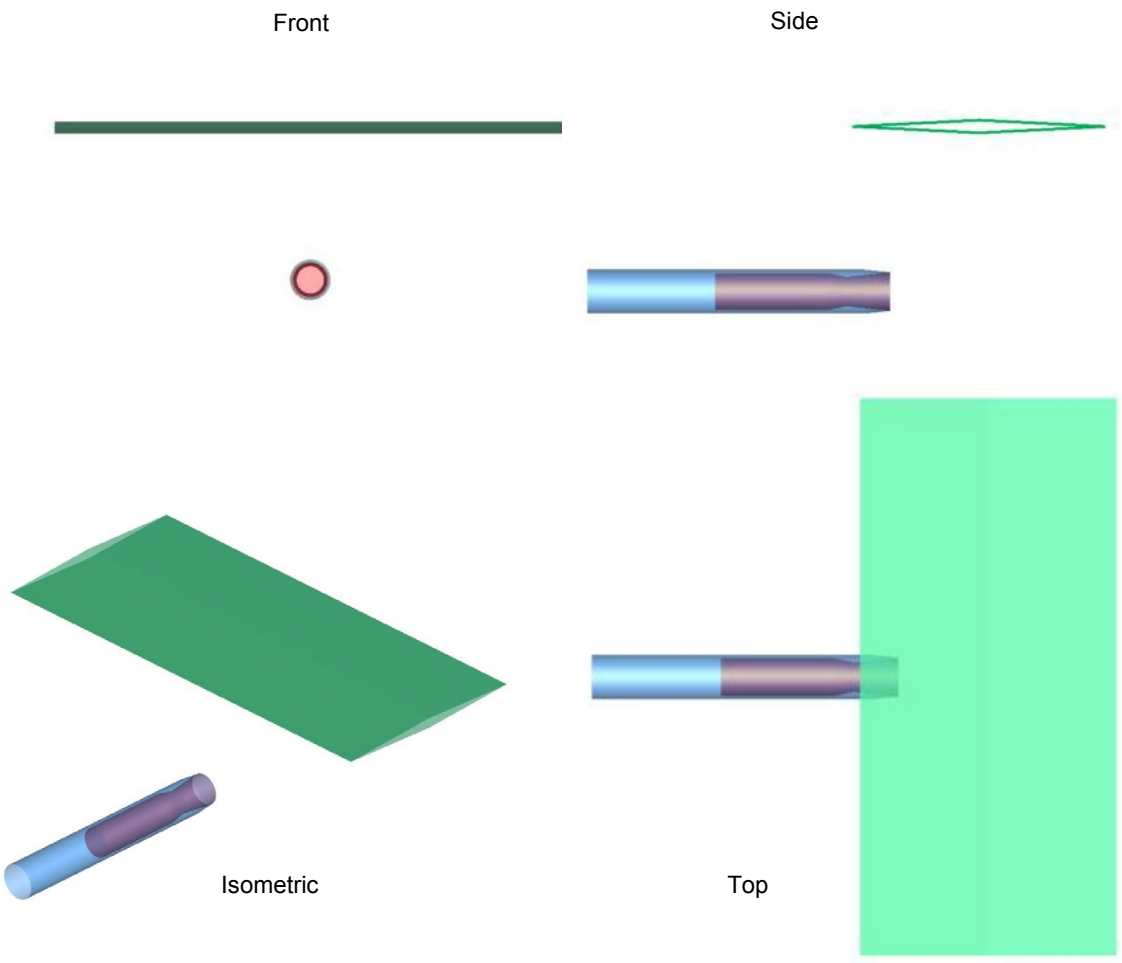

Figure 3.—Three-dimensional axisymmetric CD supersonic “Nozzle 6” with the 2.5° wedge.

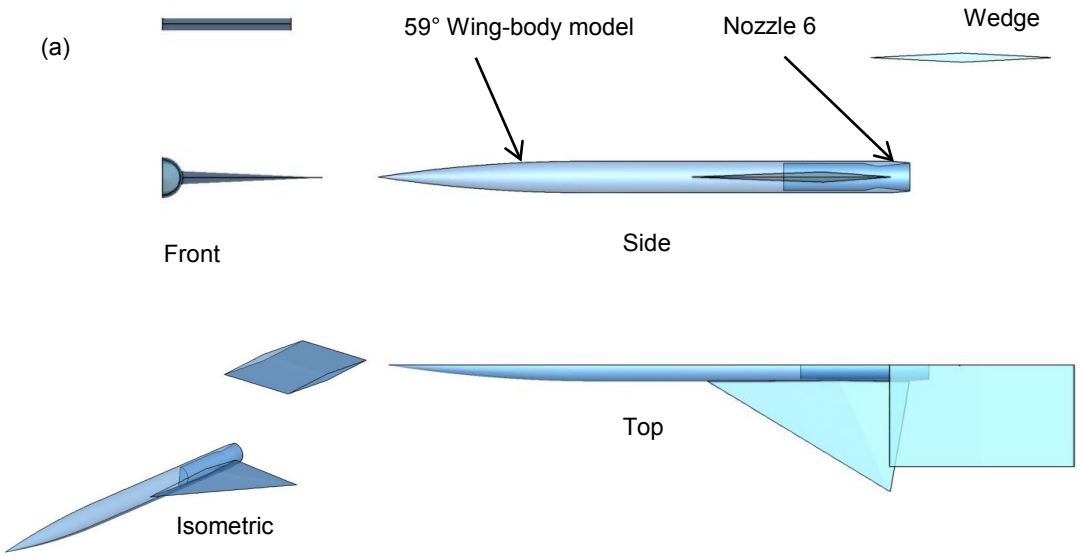

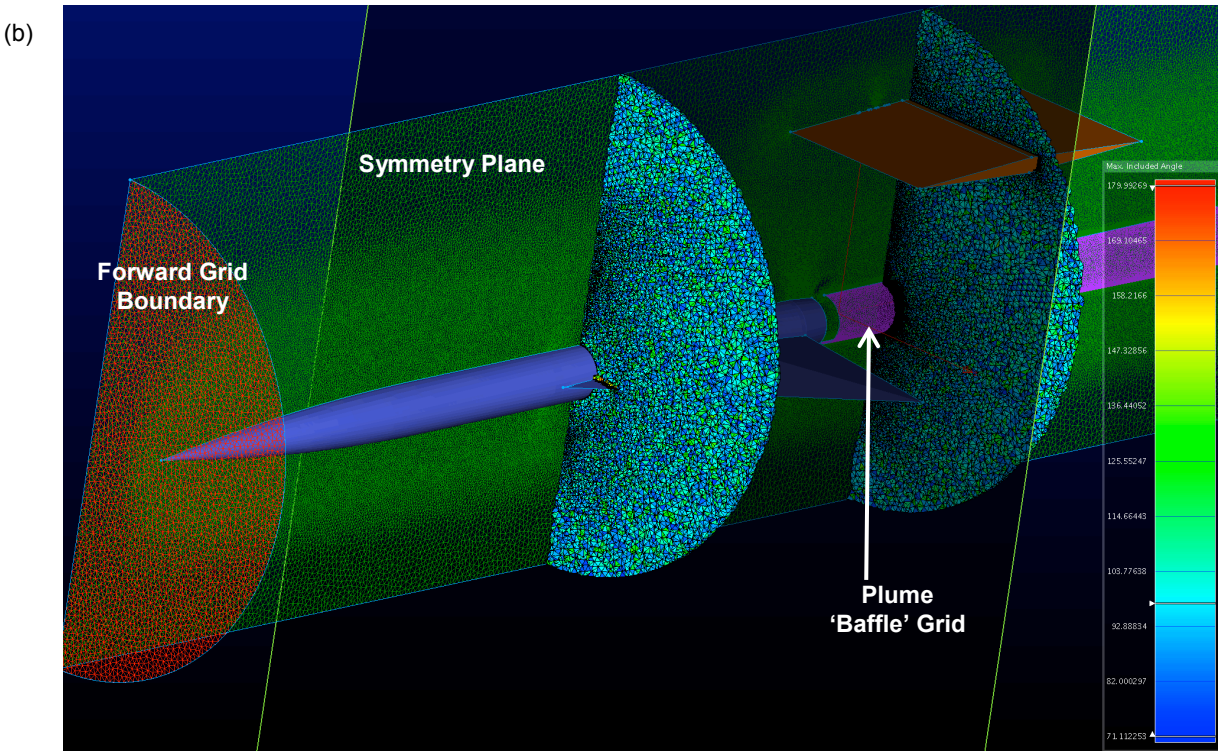

Figure 4.—(a) Cart3D and USM3D model surface of the 59° wing-body model with 'Nozzle 6' (Ref. 9). (b) USM3D grid of the 59° wing-body model with "Nozzle 6". Color contours are for the maximum included angle of each tetrahedral cell (low = 71°; high = 179°).

59° Wing-Body Model with "Nozzle 6": USM3D

A USM3D model was created for the 59° wing-body model with "Nozzle 6". Near-body grids suitable for viscous compuatations were generated for USM3D using commercial software. These near body grids were cylindrical in shape. Figure 4(b) shows grid with features such as the forward grid boundary, the symmetry plane and the nozzle plume baffle grid. The grid is highly refined near the body and a Mach cone aligned prism grid is appended to the inner cylindrical grid allow for accurate sonic boom computations at greater distances from the model.

Two cuts through the volume mesh are displayed, colored by the maximum included angle of each tetrahedral cell. The plume baffle surface grid possesses no thickness and allows for refined anisotropic cells off both sides of its surface. The baffle is cone shaped and increases in diameter by 0.5° to simulate a nozzle with an expanding jet or plume. A nozzle pressure ratio of 8.0 was used for the computations and the model length (256.66 in.) was computed in feet with a Reynolds number of 2.16 per foot, at an altitude of 50,000 ft to simulate a realistic sized supersonic vehicle in flight. The boundary conditions were set to no slip for all surface boundaries on the 59° wing-body model and the wedge, except for the nozzle lip which was set to an inviscid boundary. The nozzle plenum face was set to jet exhaust flow. The initial spacing off the solid surfaces was 0.0001 in. to provide y+ values around 1.0. The anisotropic spacing of the baffle was set to 0.01 in. and the baffle "surface" average-edge length was a factor of three smaller than the surrounding mesh. Most of the configuration had y+ values less than 1.0 except a very small region at the wing-body intersection and the leading edge (near 2.0).

Results

2-D CD Supersonic Slot Nozzle: WIND-US and PAB3D

Two-dimensional solutions with WIND-US are shown with Mach contours in Figure 5 and Figure 6, and detailed pressure distributions are shown in Figure 7. Two-dimensional solutions with PAB3D are shown with Mach contours in Figure 8. Figure 9 compares the results of the two codes.

Figure 5(a) shows the Mach number contours for the 2.5° wedge simulation in the absence of the nozzle plume, and displays the entire computational domain. Figure 5(b) shows the contours for the wedge and the 2-D CD supersonic slot nozzle plume interaction, and also displays the entire computational domain. The nozzle plume was deflected 2.5° down for the length of the wedge, and then deflected 2.5° back to the axial direction. Figure 5(c) is a close-up view of the plume interaction in Figure 5(b). At the top of the contour plot (Figure 5(c)), the shocks created by the nozzle lip interact with shocks from the wedge and a reflection from the WIND-US "freestream" boundary. This reflected shock intersects the nozzle plume.

A similar situation was observed in Figure 6(a) for the 5° wedge-only, and Figure 6(b) for the 2-D CD supersonic slot nozzle with the 5° wedge, where the nozzle plume was deflected down 5°. A closeup of the plume and shock interaction is provided. Figure 6(c) shows the Euler solution, using the same geometry and flow conditions for the 5° wedge. These figures also demonstrate how the wedge shock is displaced by a thickening of the nozzle plume (Figure 6(b)) when compared to the Euler nozzle plume (Figure 6(c)).

Both Figure 5 and Figure 5 demonstrate how the nozzle plume boundary is turned or deflected by the wedge shock. As the lower boundary turns, shocks form off the lower nozzle plume boundary and the wedge shock appears to pass through the plume.

The near field pressure signature coefficient, $\Delta P/P$, is compared in Figure 7(a) along a line located 12.5 in. below the nozzle centerline for five cases: (1) 5° wedge with cold jet, (2) 2.5° wedge with cold jet, (3) 5° wedge with 1900 °R jet (4) 5° wedge only, and (5) 2.5° wedge only. For the 2.5° wedge shock, the maximum $\Delta P/P$ of 0.179 was at x=181 in. The magnitude for the 2.5° wedge shock with the nozzle plume was 8.2 percent higher than the magnitude without the nozzle plume. For the 5° wedge shock the maximum $\Delta P/P$ of 0.381 was at x=177 in. The maximum value of $\Delta P/P$ was the same for both a cold and

hot (1900 °R) jet. The difference between the 5° wedge shock with and without the jet was 5.5 percent. For both cases, the presence of a viscous nozzle plume slightly increases the peak over-pressure, due to the increased turning angle caused by the thickened viscous nozzle plume. The small shocks seen at x=220 in. are caused by the reflection of the nozzle lip shock off the "freestream" boundary, which are not present for the wedge-only case.

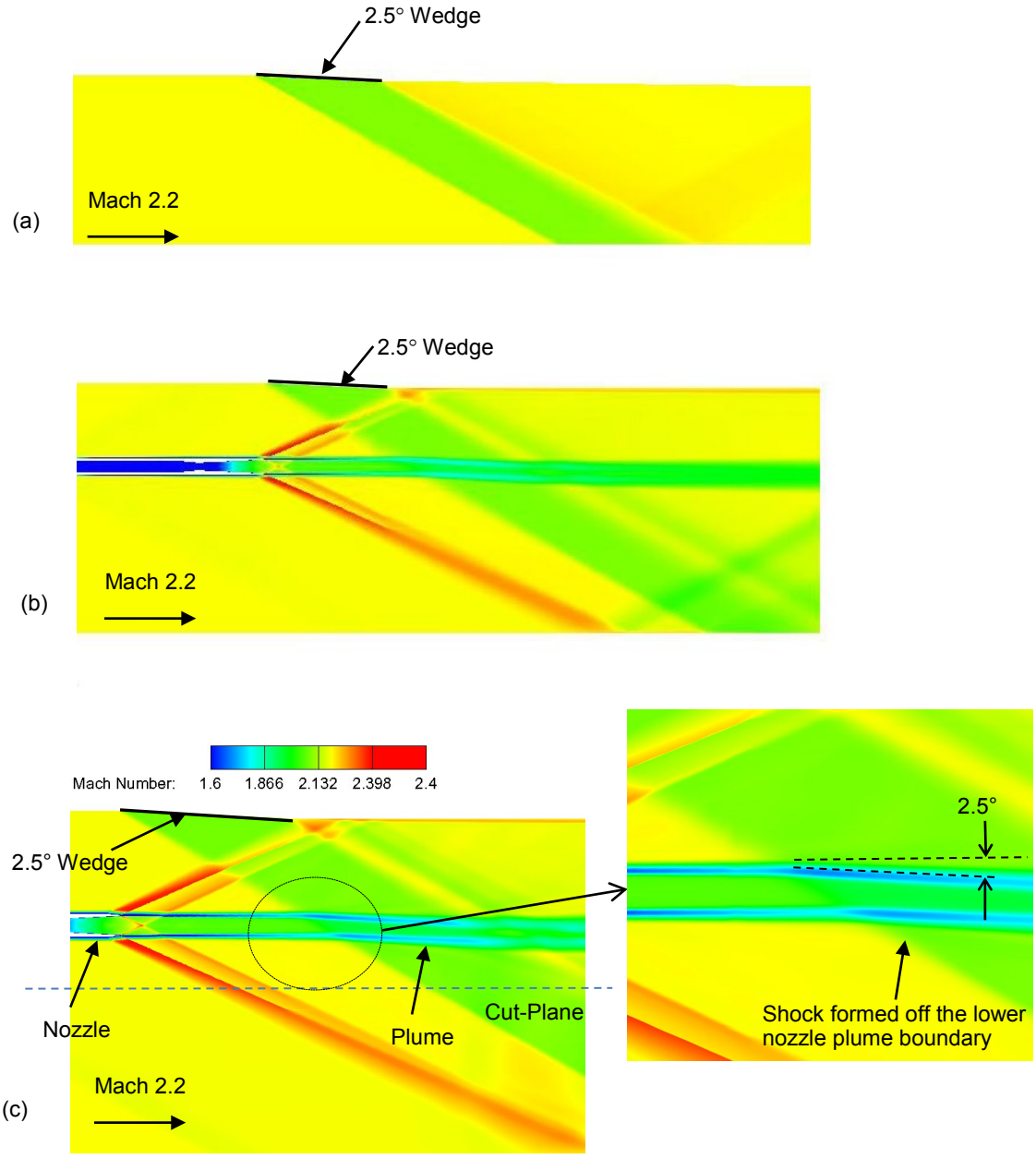

Figure 5.—WIND-US Mach contours for 2.5° wedge angle, (a) wedge-only, (b) full computational domain of the 2-D CD supersonic slot nozzle at NPR = 8, (c) close-up of the 2-D CD supersonic slot nozzle at NPR = 8. Shows the location of the cut plane for ΔP/P data at y=-12.5 in.

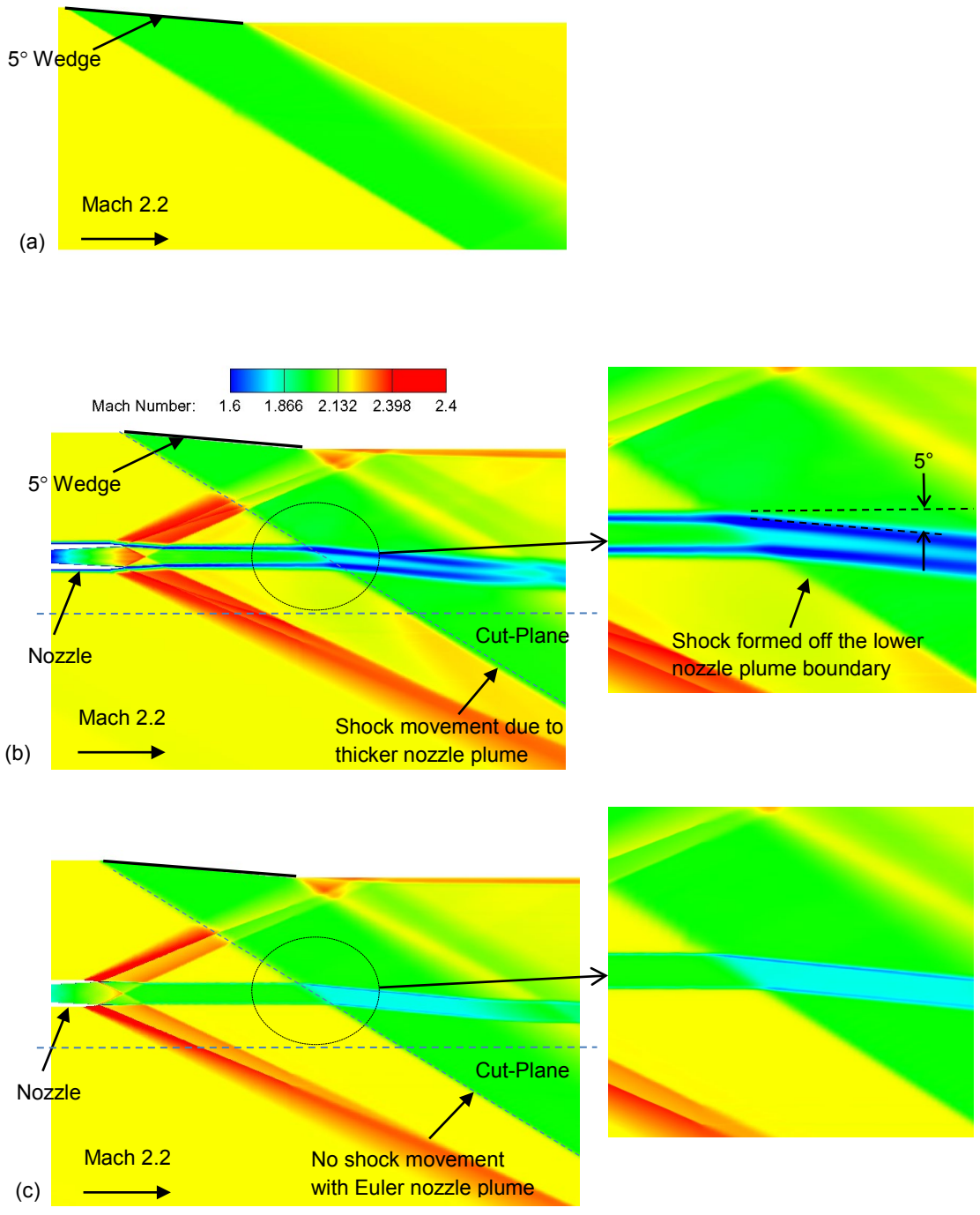

Figure 6.—WIND-US Mach contours for 5° wedge angle, (a) wedge-only, (b) 2-D CD supersonic slot nozzle at NPR = 8, (c) 2-D CD supersonic slot nozzle Euler solution.

Figure 7(b) compares pressure signatures for the 2.5° wedge simulation, at a location of 12.5 in. below the nozzle centerline. WIND-US simulations were conducted with (1) a viscous boundary layer using the SST turbulence model, (2) an inviscid (Euler) solution, and (3) a viscous solution of the wedge-only. The pressure profile for the Euler solution is indistinguishable from the 2.5° wedge-only case, except for the expected differences due to reflection of the nozzle lip shocks. For the turbulent case, the wedge shock moved slightly upstream due to the thicker viscous nozzle plume. The additional flow

turning caused a change in wedge shock location. Figure 7(c) shows the same comparison of (1) turbulent, (2) Euler, and (3) wedge-only pressure signatures for the 5° wedge. The Euler case resembles the 5° wedge only case, based on agreement in the plateau between x=180 and x=190. However, the Euler case more closely resembles the turbulent cases based on the the peak value and the shock location.

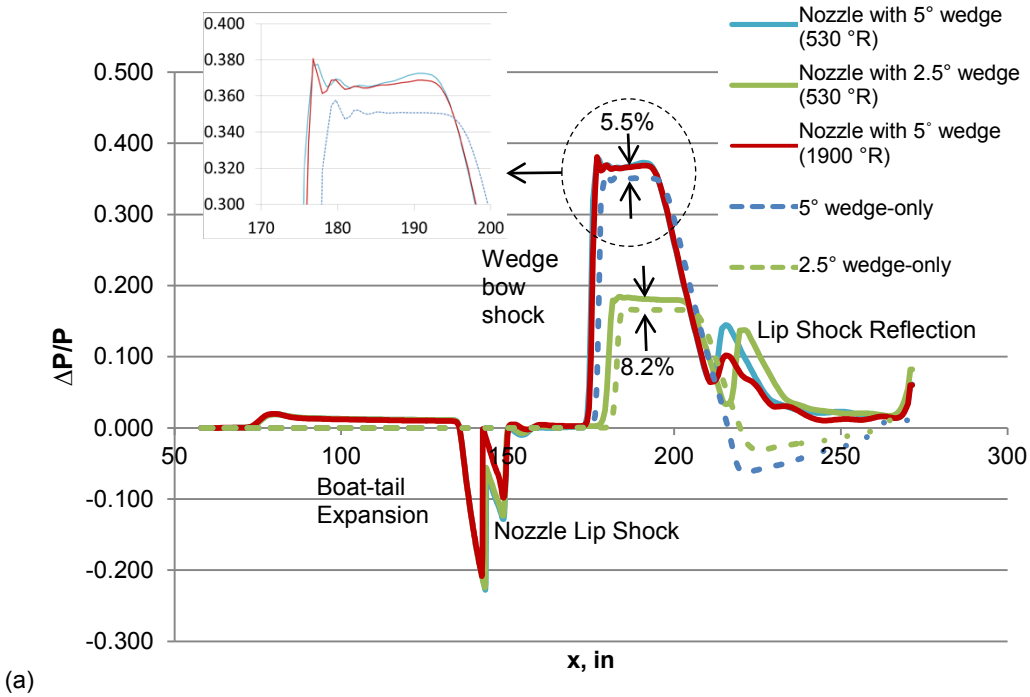

(a)

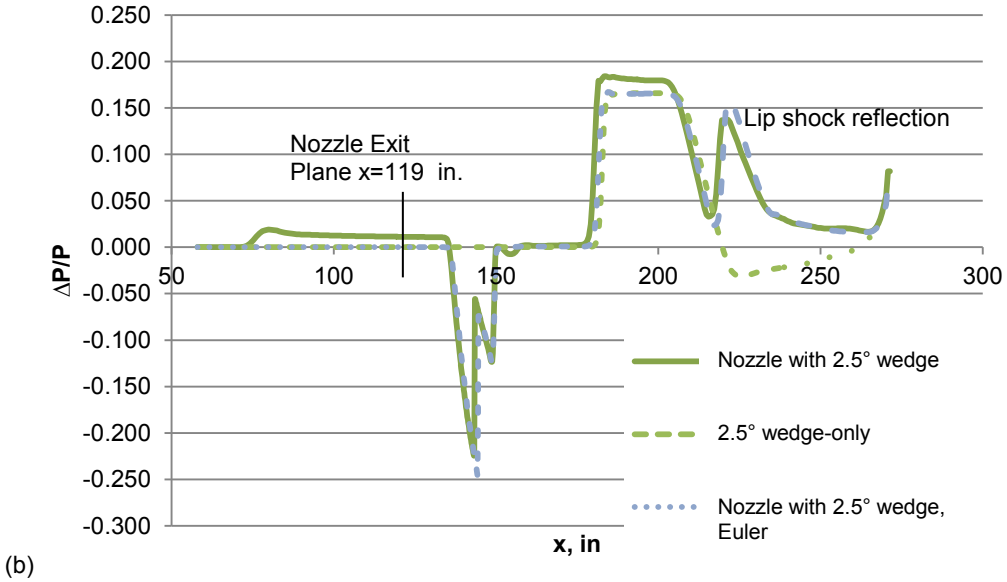

(b)

Figure 7.—(a)WIND-US ΔP/P at 12.5 in. below nozzle centerline for 2.5° and 5° wedge angle. Wedge-only, and 2-D CD supersonic slot nozzle NPR = 8. (b) WIND-US ΔP/P at 12.5 in. below nozzle centerline for 2.5° wedge angle. Wedge-only, and 2-D CD supersonic slot nozzle at NPR = 8, both viscous and Euler solutions. (c). WIND-US ΔP/P at 12.5 in. below nozzle for 5° wedge angle. Wedge-only, and 2-D CD supersonic slot nozzle at NPR = 8, both viscous and Euler solutions.

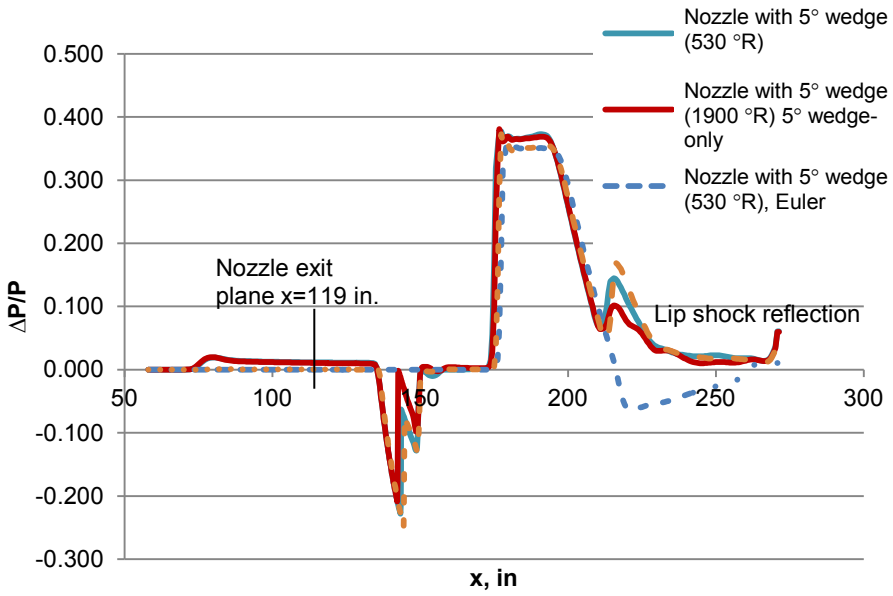

Figure 7.—Concluded.

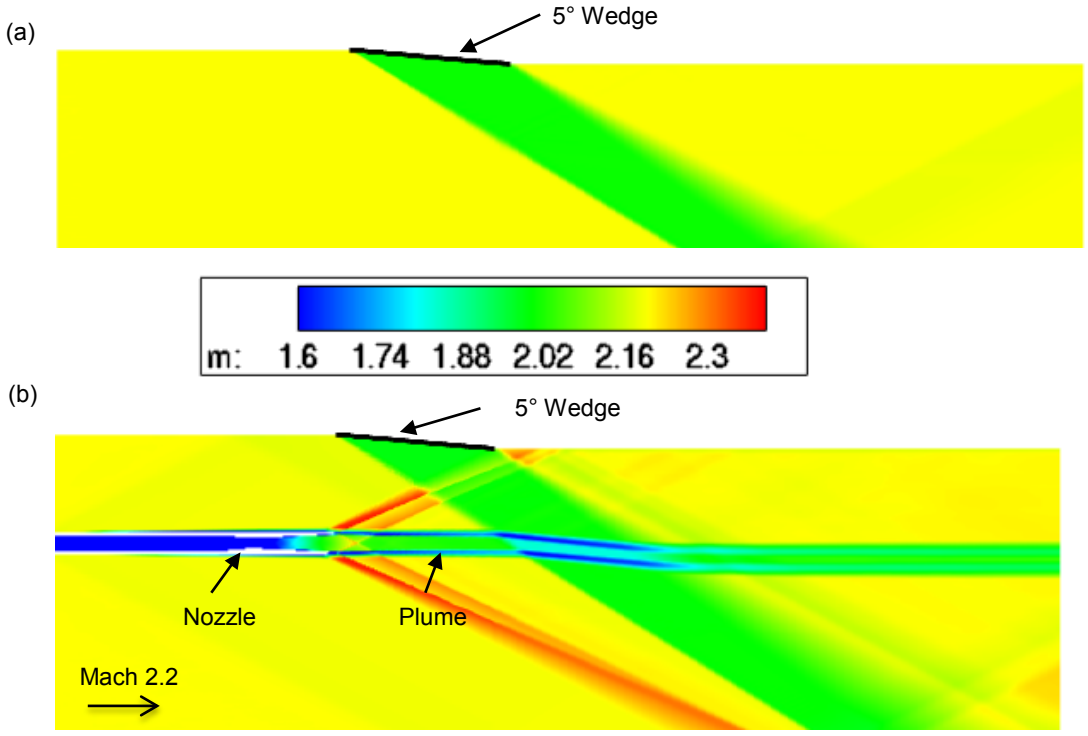

Figure 8.—PAB3D Mach contours for 5° wedge angle, (a) wedge-only, (b) with 2-D CD supersonic slot nozzle at NPR = 8

Figure 8(a) shows the PAB3D Mach number contours for the 5° wedge simulation in the absence of the nozzle plume, and Figure 8(b) shows the contours with the 5° wedge and the 2-D CD supersonic slot nozzle interaction. Similar to the WIND-US computations, the shocks created by the nozzle lip were reflected off the "freestream" boundary behind the wedge and back to the nozzle plume centerline. The PAB3D nozzle plume was deflected 5° down for the length of the generator, and then turned back 5° to

exhaust in the axial direction. The nozzle plume was shifted down from its source due to the presence of the wedge shock. PAB3D Mach contours showed good qualitative comparison with WIND-US Mach contours.

Figure 9 shows comparisons between PAB3D pressure signatures with the k-ε turbulence model, and WIND-US pressure signatures with the SST turbulence model, at a location of 12.5 in. below the nozzle centerline. This comparison demonstrates (1) that WIND-US and PAB3D obtain the same peak pressure signature for the 5° wedge-only case, and (2) obtain the same peak pressure signature for the 2-D CD supersonic slot nozzle and 5° wedge shock interaction. Discepancies between the WIND-US and PAB3D pressure profiles occur downstream of the interaction at x= 213 in. for both the wedge-only case and the nozzle plume with the 5° wedge shock. This discrepancy could be due do the difference in turbulence models (not studied), but also demonstrates the need for a comparison to experimental data.

3-D Axisymmetric CD Supersonic "Nozzle 6": WIND-US

WIND-US Mach contours on the symmetry plane for the 3-D axisymmetric CD supersonic "Nozzle 6" and the 2.5° wedge are displayed in Figure 10. This was a fully 3-D Euler simulation. The nozzle plume was first deflected down 2.5° , then deflected up 2.5° , and finally deflected back to the axial direction. Figure 11 shows the ΔP/P for the "Nozzle 6" and wedge interaction for a location one diameter (15.24 in.) below the nozzle centerline. A comparison is made between the wedge-only and "Nozzle 6" with the wedge. The nozzle boat tail expansion, lip shock and the secondary expansion/shock around the nozzle plume can be seen for values of x=70 to 100 in. The wedge bow shock interaction can be seen at x=175 in., and comparisons can be made to the wedge-only. The peak ΔP/P for the nozzle plume and wedge case was 0.31, which is 15.6 percent greater than the wedge-only. The minimum ΔP/P was –0.286, 8.3 percent less than the wedge-only.

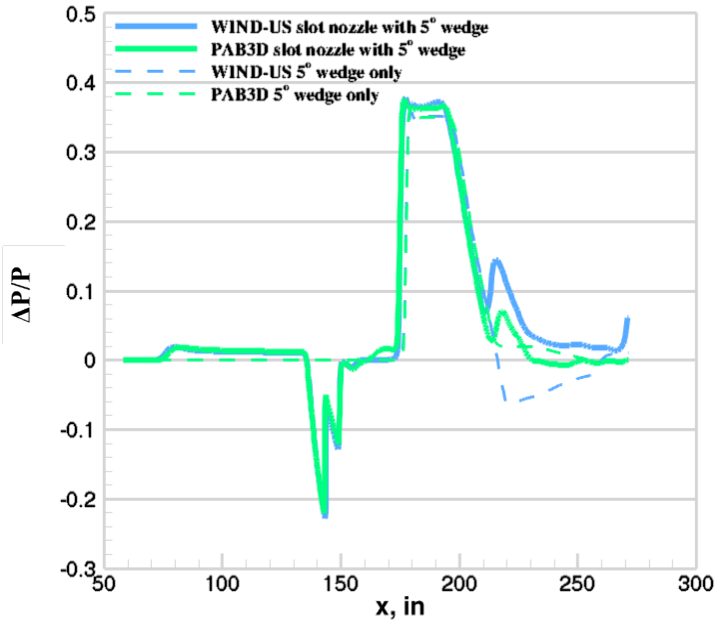

Figure 9.—Comparison between WIND-US and PAB3D ΔP/P at 12.5 in. below nozzle centerline for 5° wedge angle. Wedge-only and 2-D CD supersonic slot nozzle at NPR = 8.

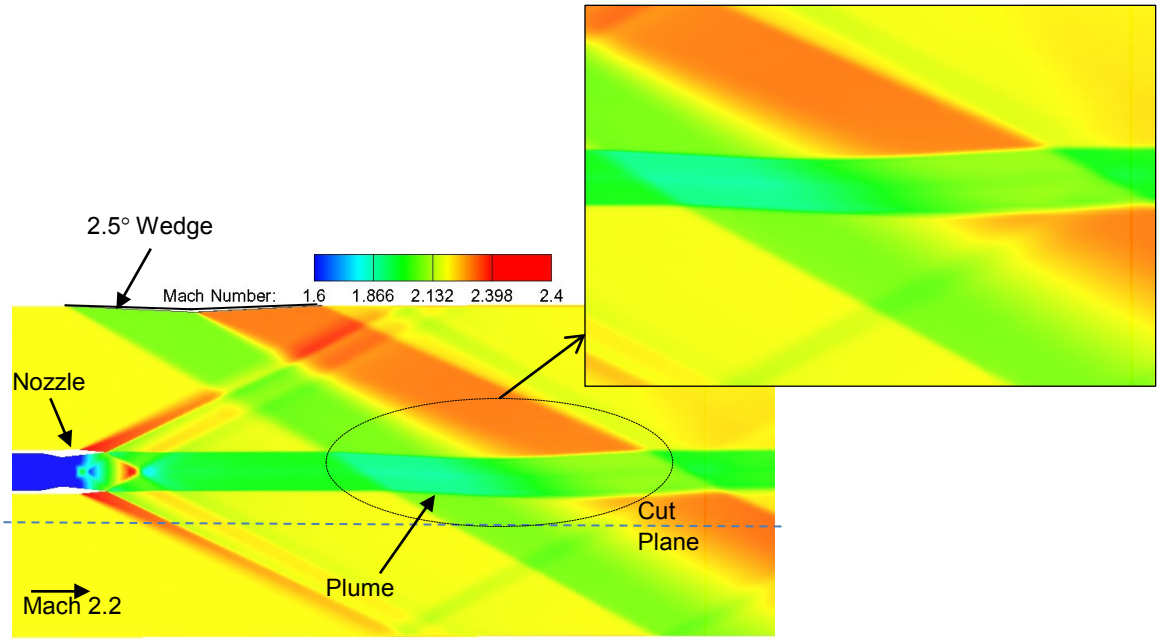

Figure 10.—Centerline cut side view of WIND-US Mach contours for 2.5° wedge angle, with 3-D axisymmetric CD supersonic “Nozzle 6” at NPR = 8.

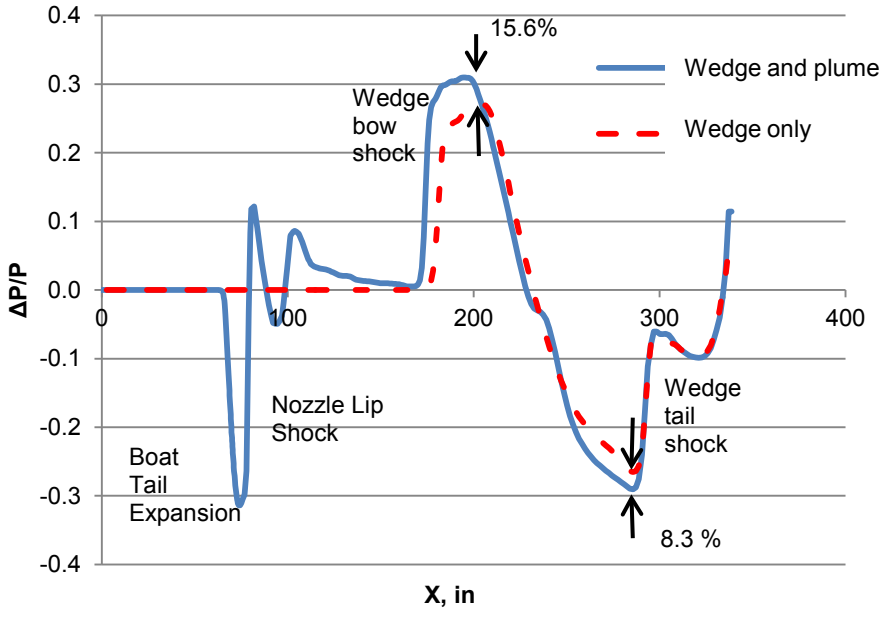

Figure 11.—ΔP/P at 15.24 in. below WIND-US solution for 2.5° wedge angle, with 3-D axisymmetric CD supersonic “Nozzle 6” at NPR = 8.

59° Wing-Body Model with "Nozzle 6": Cart3D

Figure 12(a) shows Mach number contours for the 59° wing-body model with "Nozzle 6" installed in the aft fuselage. The nozzle plume deflects downward through the compression region of the wedge and then upwards through the expansion region of the wedge before returning straight behind the vehicle. The Cart3D mesh, developed through adjoint-based mesh adaptation, is displayed in Figure 12(b). The mesh adaptation strategy included a line sensor downstream of the nozzle to generate a high density grid for the nozzle plume, in addition to both the high density grid generated around the vehicle and high density mesh aligned with vehicle shock waves. Figure 13 shows the ΔP/P signature at an h/L=1.0, a location much farther away than the previous simulations (256.6 in. versus 12.5 in.). The pressure profile was required at a larger distance from the vehicle to obtain a profile that was not affected by large changes in grid density, casued by the grid adaptation near the vehicle. The 59° wing-body model signature is present between values of x=50 and 320 in. and the wedge bow shock starts at x=350 in. The peak overpressure for the 59° wing-body model with "Nozzle 6" case was 0.10, which is 10.3 percent greater than the wedge-only. The minimum ΔP/P was –0.08, 11.3 percent more than the wedge shock. These far-field differences in ΔP/P between the 59° wing-body model with "Nozzle 6" and the wedge-only case are similar to the near-field ΔP/P results presented in the WIND-US solution (Figure 11).

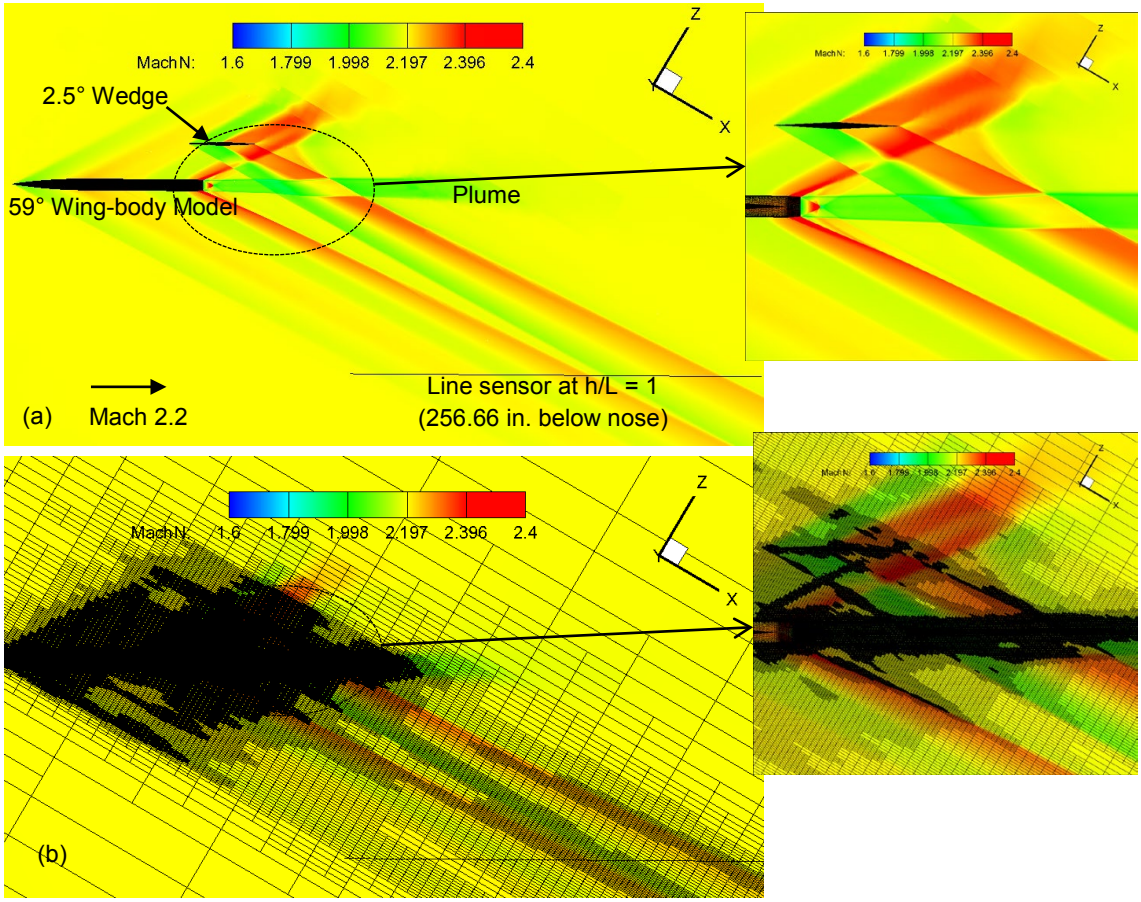

Figure 12.—(a) Cart3D Mach Contours for the 59° wing-body model with "Nozzle 6" and the 2.5° wedge; NPR = 8, (b) adapted computational mesh.

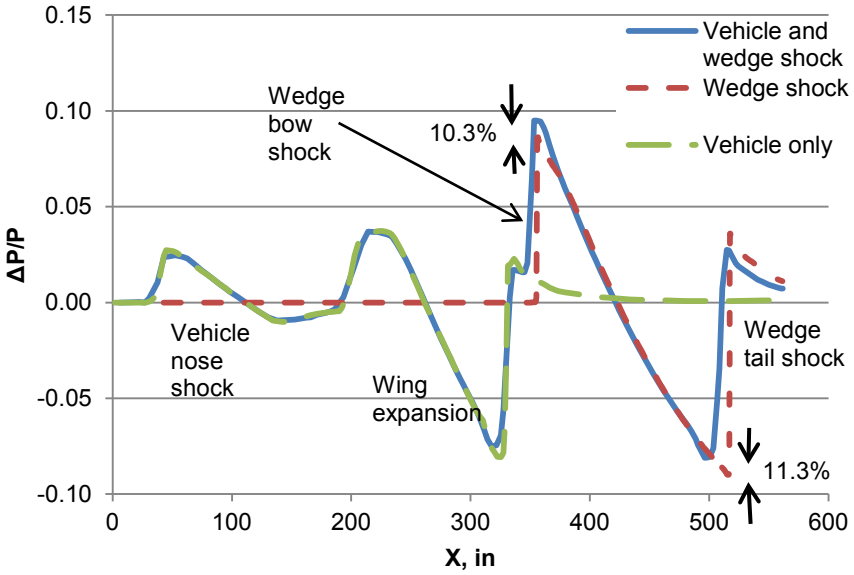

Figure 13.—Cart3D ΔP/P at h/L=1.0 for the 59° wing-body model with "Nozzle 6" and the 2.5° wedge; NPR = 8.

59° Wing-Body Model with "Nozzle 6": USM3D

A USM3D computational result of the 59° wing-body model with 'Nozzle 6' and the 2.5° wedge is shown in Figure 14(a). The plume boundary is well defined from the use of the baffle grid. The influence of the compression region of the wedge results in downward plume deflection, and upward deflection in the expansion region. The grid lines are overlaid with a view of the plume (Figure 14(b)) where the Mach cone aligned prism cells are displayed in the lower portion of the image. The cells maintain axial spacing and stretch in the Mach wave direction to reduce dissipation and attenuate the pressure signatures to greater distances. The 0.5° cone angle of the baffle does not follow the plume boundaries, but it is sufficiently close to allow for the solution of the plume boundary. The baffle grid was placed 5 in. downstream of the nozzle, but the anisotropic mesh is coarser than desired between the nozzle and initiation of the baffle clustering. The leading and trailing edges of the baffle are problematic because the anisotropic cells must make a 360° turn around the baffle, which results in stretched and enlarged cells. This was not expected to affect the pressure signature. The authors are investigating other meshing techniques to improve the mesh in this region.

Computations of the wedge-only were performed with clustering of the same baffle grid to eliminate any possible effects from different grids used in the computations. A solution of the 59° wing-body model alone was also performed with the same baffle as used with the wedge. The pressure signatures at one body length below the model nose are compared for these combinations of components in Figure 15. The wedge pressure signature was modified by the presence of the nozzle plume in a similar manner that was shown for the Cart3D Euler results (Figure 13). The wedge bow and tail shock strengths, compared to the wedge-only computation, have increased and decreased in magnitude by 15.1 and 11.3 percent, respectively, from the influence of the nozzle plume. The increased bow strength appears to be due to the downward deflection of the nozzle plume from influence of the wedge, indicating that the nozzle plume influences pressures in a similar way as a solid surface. The bow shock bends as a result of the plume and is forward of the wedge-only computation. The forward movement is due to the downward movement of the lower nozzle plume boundary. Figure 16(a) and (b) superimpose lines aligned with the bow and tail shocks from the diamond-profile computation on the symmetry plane Mach contours for solutions with and without the model and plume. The shock position deviates from linear near the center of the plume for both bow and tail shocks.

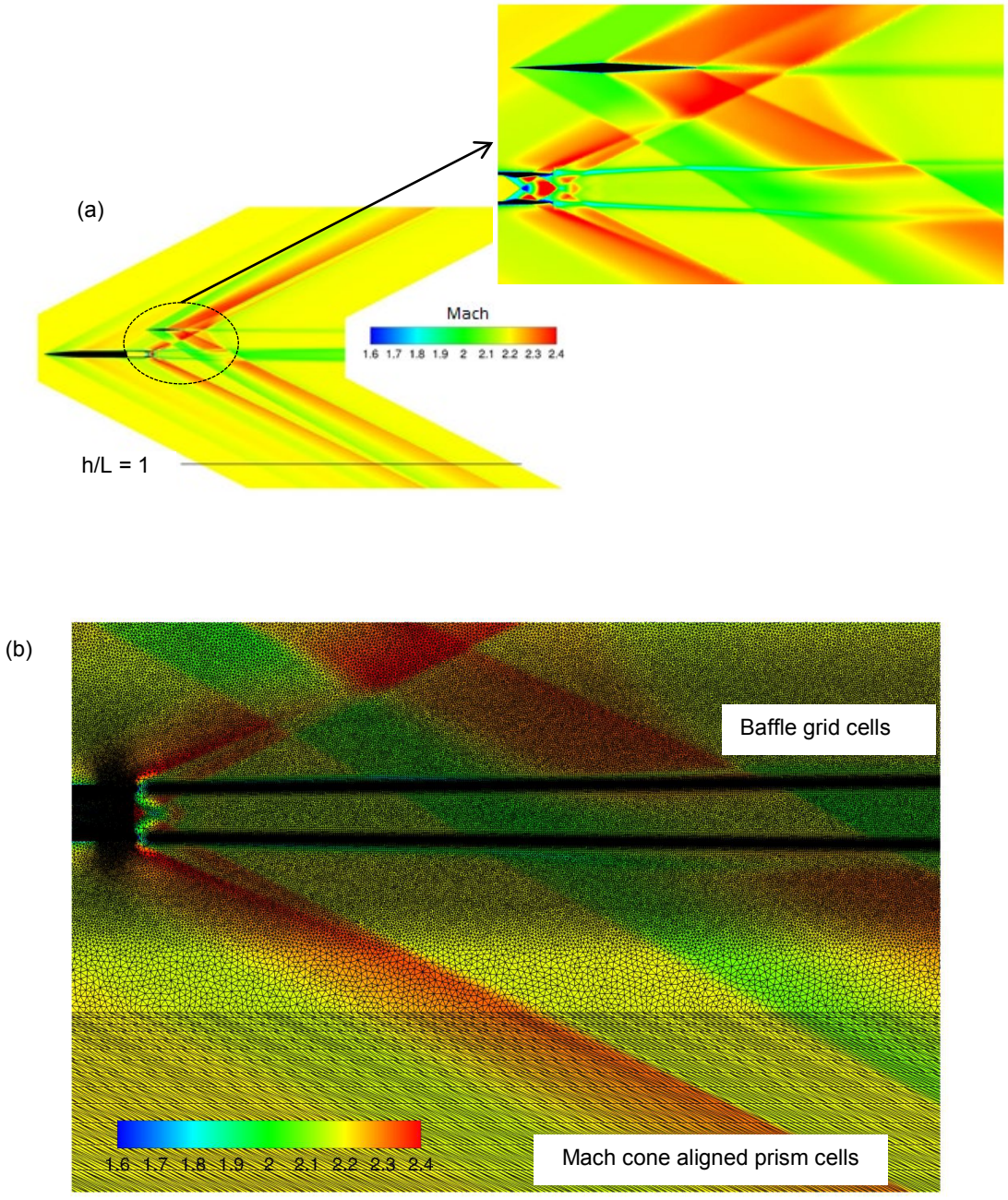

Figure 14.—(a) USM3D Mach Contours for the 59° wing-body model with “Nozzle 6” and the 2.5° wedge; NPR = 8, (b) USM3D computational mesh.

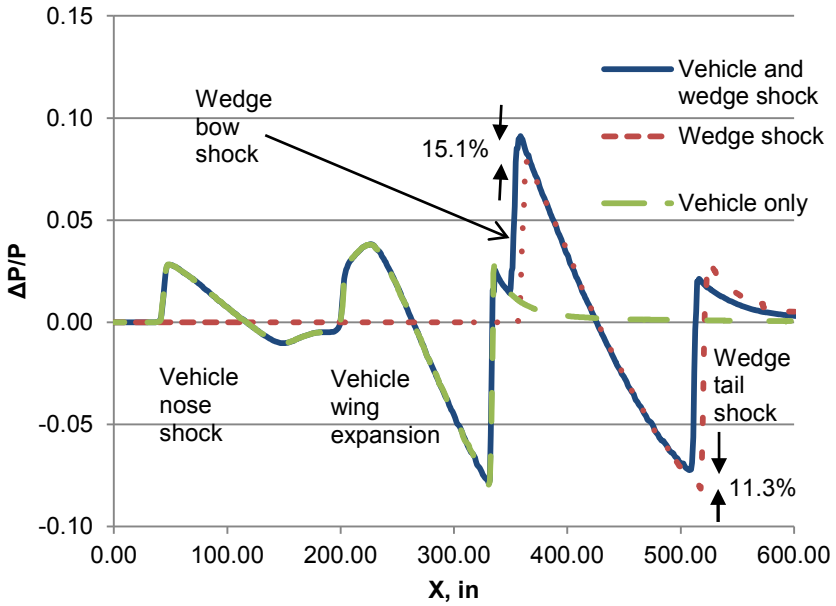

Figure 15.—USM3D ΔP/P at h/L=1.0 for the 59° wing-body model with "Nozzle 6"and the 2.5° wedge; NPR = 8.

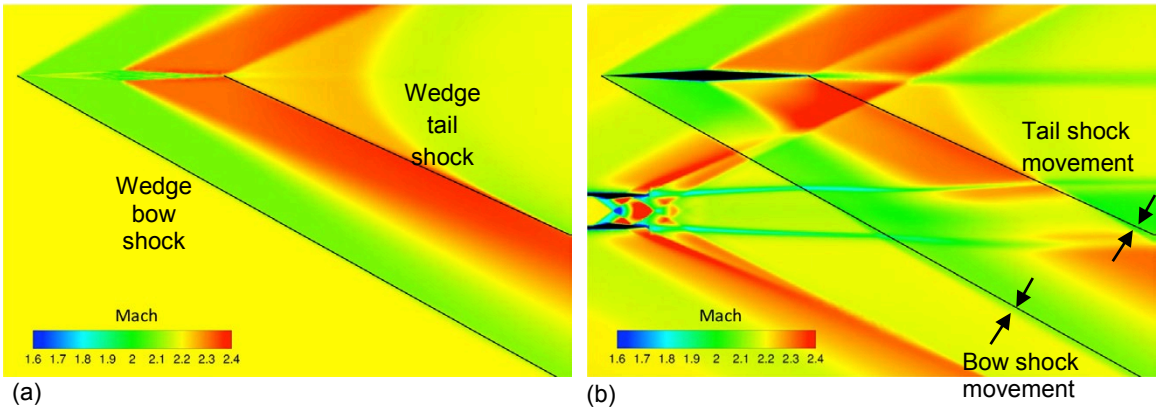

Figure 16.—USM3D 59° wing-body model with "Nozzle 6": superimposed lines aligned with the bow and tail shocks from the wedge (computation on the symmetry plane). Mach contours for solutions (a) wedge-only (b) 59° wing-body model with "Nozzle 6" and the 2.5° wedge.

Conclusions

Both 2-D and 3-D simulations were performed on exhaust nozzles with interaction from shock waves generated by a 2.5° and a 5° wedge. For 2-D nozzles, the upper nozzle plume boundary is turned or deflected by the wedge shock, and the lower boundary is also deflected through the same turning angle. As the lower plume boundary turns, shocks form off the lower boundary, parallel and co-planar to those above the boundary. Shock strength was increased by the presence of the nozzle plume at both cold and elevated nozzle plume temperatures, but increased temperature did not increase the shock strength. Results were different for turbulent CFD cases versus Euler cases, where the ΔP/P profile changed by 5.5 to 8 percent with viscous plume modeling. The 2-D inviscid case showed little difference in pressure signature with or without the presence of the nozzle plume.

The changes in the viscous computations were due to a thickened viscous nozzle plume, which increased turning of the shock, and shock strength, formed off the lower plume boundary. For design of supersonic aircraft, the effect of viscosity in the ΔP/P profile is not likely to affect the overall aircraft signature, when based on the results of the 2-D simulations. Accurate analysis of the plume and possible tailoring of the aircraft surfaces to reduce unwanted plume effects could be performed prior to closing a design. It appears reasonable to perform design studies with Euler analysis and then perform viscous CFD computations, to make high fidelity vehicle changes, before finalizing the design.

Results obtained for the 3-D simulations displayed up to a 15 percent increase in ΔP/P overpressure with the modeling of the nozzle plume (Figure 11), where the 2-D Euler results showed almost no difference with the configuration and nozzle plume (Figure 7(b)). The wedge pressure signature was modified by the presence of the plume and the plume path was modified by the pressure disturbance from the wedge. This implies that detailed computations of the nozzle plume should be modeled during design of modern low boom supersonic transport configurations. It is not clear whether these effects require viscous modeling since the trends appear to be captured with inviscid computations. It seems prudent to accurately model the plume to determine the extent of pressure signature changes during vehicle design as it is expected that different shaped vehicles could have either favorable or detrimental effects from the influence of nozzle plumes. Further study and comparison to experimental data is warranted, but at the time of publishing, no known experimental validation data exists for this shock and plume interaction. At this time, a nozzle plume and shock interaction experiment is planned for the 1- by 1-ft supersonic wind tunnel at the NASA Glenn Research Center.

References

1. Freund, D., Howe, D., Simmons, F., and Schuester, L., "Quiet Spike Prototype Aerodynamic Characteristics From Flight Test," AIAA 2008−125, Jan. 2005.
2. Graham, D., Dahlin, J., Meredith, K., and Vadnais, J., "Aerodynamic Design of Shaped Sonic Boom Demonstration Aircraft," AIAA 2005−8, Jan. 2005.
3. Putnam, L. and Capone, F., "Experimental Determination of Equivalent Solid Bodies to Represent Jets Exhausting into a Mach 2.20 External Stream," NASA TN-D-5553, 1969.
4. Castner, R. S., "Analysis of Plume Effects on Sonic Boom Signature for Isolated Nozzle Configurations," NASA/TM—2008-215414 (AIAA-2008-3729), June 2008.
5. Bui, T., "CFD Analysis of the Nozzle Jet Plume Effects on Sonic Boom Signature," AIAA-2009-1054, Jan. 2009.
6. Castner, R. S., "Slot Nozzle Effects for Reduced Sonic Boom on a Generic Supersonic Wing Section," AIAA-2010-1386, Jan. 2010.
7. Castner, R. S., "Analysis of Exhaust Plume Effects on Sonic Boom for a 59-Degree Wing Body Model," AIAA-2011-917, Jan. 2011.
8. Castner, R. S., "Exhaust Plume Effects on Sonic Boom for a Delta Wing and Swept Wing-Body Model," AIAA-2012-1033, Jan. 2012.
9. Towne, C. E., "Wind-US Users Guide, Version 2.0," NASA/TM—2009-215804, Oct. 2009.
10. Abdol-Hamid, K., Pao, S. P., Hunter, C., Deere, K. A., Massey, S. J., and Elmiligui, A. " PAB3D: Its History in the Use of Turbulence Models in the Simulation of Jet and Nozzle Flows," AIAA-2006-489, Jan. 2006.
11. Massey, S. J., POST Code Manual, URL: http://www.asm-usa.com/PAB3D/doc/post/ [cited 5 Oct. 2012].
12. Aftosmis, M. J., Berger, M. J., and Melton, J. E., "Robust and Efficient Cartesian Mesh Generation for Component-Based Geometry," AIAA Journal, Vol. 36, No. 6, 1998, pp. 952-960.
13. Aftosmis, M. J., Berger, M. J., and Adomavicius, G., "A Parallel Multilevel Method for Adaptively Refined Cartesian Grids with Embedded Boundaries," AIAA Paper 2000-0808, 38th Aerospace Sciences Meeting and Exhibit, Reno, NV, Jan. 2000.

14. Aftosmis, M. J.; and Berger, M. J., "Multilevel Error Estimation and Adaptive H-Refinement for Cartesian Meshes with Embedded Boundaries," AIAA Paper 2002-0863, 40th AIAA Aerospace Sciences Meeting and Exhibit, Reno, NV, Jan. 2002.
15. Nemec, M., and Aftosmis, M. J., "Adjoint Error-Estimation and Adaptive Refinement for Embedded-Boundary Cartesian Meshes," AIAA Paper 2007-4187, 18th AIAA CFD Conf., Miami, FL, Jun. 2007.
16. Nemec, M., Aftosmis, M. J., and Wintzer, M., "Adjoint-Based Adaptive Mesh Refinement for Complex Geometries," AIAA Paper 2008-0725, Jan. 2008.
17. Wintzer, M., Nemec, M., and Aftosmis, M., "Adjoint-Based Adaptive Mesh Refinement for Sonic Boom Prediction," AIAA-2008-6593, Aug. 2008.
18. Cliff, S. E., Thomas, S. D., McMullen, M. S., Melton, J.E., and Durston, D. A., "Assessment of Unstructured Euler Methods for Sonic Boom Pressure Signatures Using Grid Refinement and Domain Rotation Methods," NASA/TM—2008-214568, Sept. 2008.
19. Aftosmis, Michael, Nemec, Marian, and Cliff, Susan, "Adjoint-Based Low-Boom Design with CART3D (Invited), AIAA-2011-3500, 29th AIAA Applied Aerodynamics Conference, HI, Jun. 2011.
20. Elmiligui, Alaa, Cliff, Susan, Aftosmis, Michael, Nemec, Marian, Parlette, Edward, Wilcox, Floyd, and Bangert, Linda, "Sonic Boom Computations for a Mach 1.6 Cruise Low Boom Configuration and Comparisons with Wind Tunnel Data (Invited), AIAA-2011-3496, 29th AIAA Applied Aerodynamics Conference, HI, Jun. 2011.
21. Elmiligui, A., Cliff, S., Wilcox, F., and Thomas, S. "Numerical Predictions of Sonic Boom Signatures for Straight Line Segmented Leading Edge Model", Seventh International Conference on Computational Fluid Dynamics, ICCFD7-2004, Big Island, HI, Jul. 9-13, 2012.
22. Frink, N. T., Pirzadeh, S. Z., Parikh, P. C., Pandya, M. J., and Bhat, M. K., "The NASA Tetrahedral Unstructured Software System," The Aeronautical Journal, Vol. 104, No. 1040, Oct. 2000, pp. 491-499.
23. Frink, N. T., "Assessment of an Unstructured-Grid Method for Predicting 3-D Turbulent Viscous Flows," AIAA Paper-96-0292, Jan. 1996.
24. Abdol-Hamid, K. S., Frink, N. T., Deere, K. A., and Pandya, M. J.: "Propulsion Simulations Using Advanced Turbulence Models with the Unstructured-Grid CFD Tool, TetrUSS," AIAA 2004-0714, Jan. 2004.
25. Deere, K., Elmiligui, A., Abdol-Hamid K., "USM3D Simulations of Saturn V Plume Induced Flow Separation" AIAA-2011-1055, Jan. 2011.

REPORT DOCUMENTATION PAGE	Form Approved OMB No. 0704-0188

1. REPORT DATE *(DD-MM-YYYY)*	2. REPORT TYPE	3. DATES COVERED *(From - To)*
01-02-2013	Technical Memorandum	

4. TITLE AND SUBTITLE
Exhaust Nozzle Plume and Shock Wave Interaction

5a. CONTRACT NUMBER

5b. GRANT NUMBER

5c. PROGRAM ELEMENT NUMBER

6. AUTHOR(S)
Castner, Raymond, S.; Elmiligui, Alaa; Cliff, Susan

5d. PROJECT NUMBER

5e. TASK NUMBER

5f. WORK UNIT NUMBER
WBS 984754.02.07.03.13.05

7. PERFORMING ORGANIZATION NAME(S) AND ADDRESS(ES)
National Aeronautics and Space Administration
John H. Glenn Research Center at Lewis Field
Cleveland, Ohio 44135-3191

8. PERFORMING ORGANIZATION REPORT NUMBER
E-18612

9. SPONSORING/MONITORING AGENCY NAME(S) AND ADDRESS(ES)
National Aeronautics and Space Administration
Washington, DC 20546-0001

10. SPONSORING/MONITOR'S ACRONYM(S)
NASA

11. SPONSORING/MONITORING REPORT NUMBER
NASA/TM-2013-217838

12. DISTRIBUTION/AVAILABILITY STATEMENT
Unclassified-Unlimited
Subject Categories: 01, 02, and 07
Available electronically at http://www.sti.nasa.gov
This publication is available from the NASA Center for AeroSpace Information, 443-757-5802

13. SUPPLEMENTARY NOTES

14. ABSTRACT
Fundamental research for sonic boom reduction is needed to quantify the interaction of shock waves generated from the aircraft wing or tail surfaces with the exhaust plume. Both the nozzle exhaust plume shape and the tail shock shape may be affected by an interaction that may alter the vehicle sonic boom signature. The plume and shock interaction was studied using Computational Fluid Dynamics simulation on two types of convergent-divergent nozzles and a simple wedge shock generator. The nozzle plume effects on the lower wedge compression region are evaluated for two- and three-dimensional nozzle plumes. Results show that the compression from the wedge deflects the nozzle plume and shocks form on the deflected lower plume boundary. The sonic boom pressure signature of the wedge is modified by the presence of the plume, and the computational predictions show significant (8 to 15 percent) changes in shock amplitude.

15. SUBJECT TERMS
Exhaust nozzles; Plumes; Shock wave interaction

16. SECURITY CLASSIFICATION OF:			17. LIMITATION OF ABSTRACT	18. NUMBER OF PAGES	19a. NAME OF RESPONSIBLE PERSON
a. REPORT	b. ABSTRACT	c. THIS PAGE			STI Help Desk (email:help@sti.nasa.gov)
U	U	U	UU	28	19b. TELEPHONE NUMBER *(include area code)* 443-757-5802